

# Scatter and Heat Conduction Correction Factors for Two Glass Vessel Geometries in Sealed Water Calorimeters

H. Palmans<sup>a</sup>, M. Defloor<sup>b</sup>, S. Benmokhtar<sup>a</sup>, I. Stoker<sup>a</sup> and K. Rosser<sup>a†</sup>

<sup>a</sup>National Physical Laboratory, Middlesex, UK

<sup>b</sup>Ghent University, Gent, Belgium

## Abstract

Two perturbations are associated with the use of glass vessels to seal high-purity water in sealed water calorimeters: one for scatter and attenuation of the radiation field and a second one for excess heat flowing towards the measurement point. Both perturbations have been investigated here to some extent. A set of Domen-type glass vessels with various diameters and wall thicknesses is used to systematically measure the scatter and attenuation effect and the results are compared with Monte Carlo calculations. Four vessels out of the same set were used to measure their relative response in a <sup>60</sup>Co beam and to compare these results with finite element simulations of excess heat. A simulation of excess heat for a standard NPL vessel, which will be used in <sup>60</sup>Co is performed as well.

## 1. Introduction

Since Domen proposed a design of a sealed water calorimeter (SWC) [1, 2], various investigators and standard dosimetry laboratories have adopted a similar approach. In this, high-purity water, usually saturated with argon, hydrogen or a hydrogen/oxygen mixture, is contained in a small vessel to seal it from the water phantom, which contains water with a lower purity. The high-purity water is needed for controlling the chemical heat defect. If properly designed, the vessels induce only small perturbation effects and thus require small corrections, which can be determined with acceptably small uncertainties. Nevertheless, the corrections are substantial enough for a primary standard to justify a thorough investigation and it is worth performing a systematic investigation yielding generic formulae as a function of vessel dimensions and/or energy for those correction factors. Two SWC vessel geometries are generally used for photon beams: the Domen- or cigar-type and the pancake-type. In the Domen-type geometry [1, 2], which is used in many laboratories (see table 1 below for references), a cylindrical vessel is positioned perpendicular to the beam direction and the thermistors are normally positioned on the axis. In the pancake type, which is used at NPL and PTB, a cylindrical vessel with two parallel flat faces is positioned with its axis coinciding with the beam axis. Two perturbations are due to the presence of a glass vessel: firstly, the perturbation of the radiation field at the point of measurement due to the change in scatter conditions and due to attenuation of the primary beam and secondly, the perturbation due to an excess temperature rise in the glass vessel which produces excess heat to flow towards the point of measurement.

Since the scatter and attenuation perturbation at the point of measurement is usually small, a number of groups developing water calorimeters have just ignored the effect. Others have done Monte Carlo simulations and/or measurements to determine correction factors for vessel induced scatter and attenuation. An overview of values for <sup>60</sup>Co found in the literature is given in table 1, showing corrections generally not larger than 0.2%. Determinations for medium-energy x-rays with voltage potentials between 100 kV and 250 kV were reported by

---

<sup>†</sup> Present address: Parkside Hospital, London, UK

Seuntjens et al. [7] who calculated values between 0.998 and 1.000 for a 40 mm diameter PMMA vessel with a wall thickness of 0.5 mm using the Monte Carlo method. A few determinations in high-energy photon beams have been reported as well. Seuntjens et al. [4] measured a value of  $1.0015 \pm 0.0002$  in a 20 MV photon beam for the 67 mm diameter, 0.9 mm thick glass vessel used at the National Research Council, Canada. For the same or similar vessels, values ranging from 1.0026 to 0.9994 were measured in photon beams with nominal accelerator potentials between 10 MV and 30 MV [8]. More recently, measurements were performed in a number of clinical high-energy photon beams by the NMI in the Netherlands and Belgium, yielding values between 1.0023 and 1.0004 for beams with beam qualities  $\%dd(10)_x$  in the range of 68% to 82% [6].

Table 1. Scatter and attenuation correction factors,  $k_{sc}$ , with standard uncertainties for Domen-type glass vessels in  $^{60}\text{Co}$  from the literature (MC = Monte Carlo, Exp = Experimental, IC = Ion chamber,  $\emptyset$  is the diameter of the vessel and  $t_{wall}$  the thickness of the cylindrical vessel wall).

Vessel properties			$k_{sc}$	Method	Ref
Material	$\emptyset$ (mm)	$t_{wall}$ (mm)			
Glass	33	0.25 <sup>(*)</sup>	$1.0014 \pm 0.0010$	Exp - IC	[2]
PMMA	40	0.5	$1.0000 \pm 0.0012$ <sup>(o)</sup>	MC	[3]
Glass	67	0.9	$1.0021 \pm 0.0005$	Exp - IC	[4]
Glass	67	0.9	$1.0028 \pm 0.0008$	MC	[4]
Glass	40	0.4 <sup>(*)</sup>	$1.0005 \pm 0.0010$	Exp: diamond	[5]
Glass	40	0.5	$1.0012 \pm 0.0010$	MC	[5]
Glass	40	1.0	$1.0024 \pm 0.0008$	MC	[5]
PMMA	40	0.5	$1.0000 \pm 0.0010$	MC	[5]
Glass	73	0.73	$1.0019 \pm 0.0006$	Exp.: IC	[6]

<sup>(o)</sup> No value was given, only a maximum correction of 0.2%

<sup>(\*)</sup> This is the wall thickness in the longitudinal centre of the vessel, which was not constant in thickness

The effect of excess heat generated in the glass material of the thermistor probes and the vessel has been studied by several investigators. Concerning the effect of the thermistor probes there is a general agreement that the effect can be reduced below 0.1% by reducing the diameter of the probes to 0.4 mm and starting the fitting of post-irradiation drift curves 10 to 20 s after the end of the irradiation [2, 4, 5, 9-14]. The effect of the vessel on the other hand is not always negligible and calculated corrections as well as some experimental support has been reported in various publications. Numerical heat conduction simulations were performed to obtain time dependent post-irradiation corrections that can be used to correct measured post-irradiation drift curves [2, 4, 5, 9-14]. Alternatively correction factors are calculated for the results from extrapolation to mid-run when the drift curves remain uncorrected. These corrections are usually not larger than 0.5% [4, 5, 10]. Very few experimental efforts to study these effects have been reported. Krauss and Roos compared post-irradiation drift curves for some thick-walled PMMA vessels with the results from numerical simulations using ANSYS [9] and Krauss compared measured and calculated post-irradiation drift curves for glass vessels of the pancake-type [14]. Palmans [12] compared post-irradiation drift curves for some thick-walled Dömen-type glass vessels of glass with the results from numerical calculations and also compared the relative response of the calorimeter using three different vessel dimensions with the relative response resulting from the calculations.

In this work, a set of Dömen-type glass vessels with various diameters and wall thicknesses is used to systematically measure the relative effects of both perturbations and the results are

compared with Monte Carlo calculations and numerical simulations of heat transfer. This is essentially a continuation of the work of Palmans [12]. For the pancake type, the work is restricted to numerical calculation of excess heat.

## 2. Materials and methods

The general operational features of the water calorimeter systems used for the experiments are described in other papers. The Ghent University water calorimeter is described and discussed in detail by Seuntjens and Palmans [5]. It is based on the principles of Domen's calorimeter [2] with the main exception that it operates at 4°C in order to remove any concern related to convection. The calorimeter tank is a 30 cm × 30 cm × 30 cm water phantom thermally isolated by styrofoam. Isolation of the wooden enclosure with dimensions of 85 cm × 85 cm × 85 cm allows temperature stabilization of the air surrounding the calorimeter phantom. The temperature increase due to irradiation is measured at the centre of a cylindrical vessel using small thermistors that are embedded in the tip of small glass probes. The probes consist of commercially available thermistors embedded in glass rods with a diameter of 0.5 mm. The standard vessel has a diameter of 4 cm, a length of 14 cm and a wall thickness varying from 0.4 mm in the central part corresponding with the central axis of the beam to 1.6 mm at the lateral edges. The resistance of the thermistors is measured by connecting them in a one-armed AC bridge powered by two equal oscillator signals in counter-phase. The NPL water calorimeter assembly has been described by Williams and Rosser [15]. The calorimeter phantom is a double walled PMMA tank and the temperature-stabilized refrigerant is flowing between the two walls at all sides of the water phantom except for a 15 cm diameter entrance window. The thermistor probes are of similar design as in the Ghent calorimeter and the glass vessels are pancake-type vessels with a 0.8 to 1.0 mm thick entrance window and 4 mm walls at all other sides. Both thermistors are connected to separate AC bridges such that both signals could be used as the other's verification and such that measurements can go on if one thermistor fails.

### 2.1. Scatter effects

#### 2.1.1. Monte Carlo simulations

Monte Carlo simulations were performed using the EGSnrc code system [16]. The simulated geometry is shown in figure 1. The  $^{60}\text{Co}$  beam was simplified to a parallel mono-energetic photon beam with energy 1.25 MeV and a square field parallel beam. The phantom material was water (liquid water as defined in ICRU report 37 [17]) and the dimensions extended to 5 cm between the beam and the centre of the sensitive volume and 15 cm in all other directions from the centre of the sensitive volume. The sensitive volume was a 3 mm diameter and 20 mm long cylinder, orientated perpendicular to the beam axis. The glass vessel was defined by two cylinders, perpendicular to the beam axis and with a length equalling the phantom size in that direction. The material was pyrex (borosilicate glass as defined in ICRU report 37). The scatter and attenuation correction factor was obtained as the ratio of the dose in the sensitive volume in the absence of the vessel and the dose in the presence of the vessel. Though we are aware that a correlated sampling technique could probably reduce the calculation time for obtaining a certain statistical uncertainty, the required cpu time was not a real issue and no attempt was made to implement correlated sampling. We also assume that all the simplifications we made compared with the real  $^{60}\text{Co}$  beam have a negligible effect on the small corrections. The dimensions of the vessel ranged from 10 to 50 mm for the radius,  $r_{\text{vessel}}$ , and 1 to 4 mm for the wall thickness,  $t_{\text{wall}}$ . The size of the square field varied between 4 cm × 4 cm and 12 cm × 12 cm.

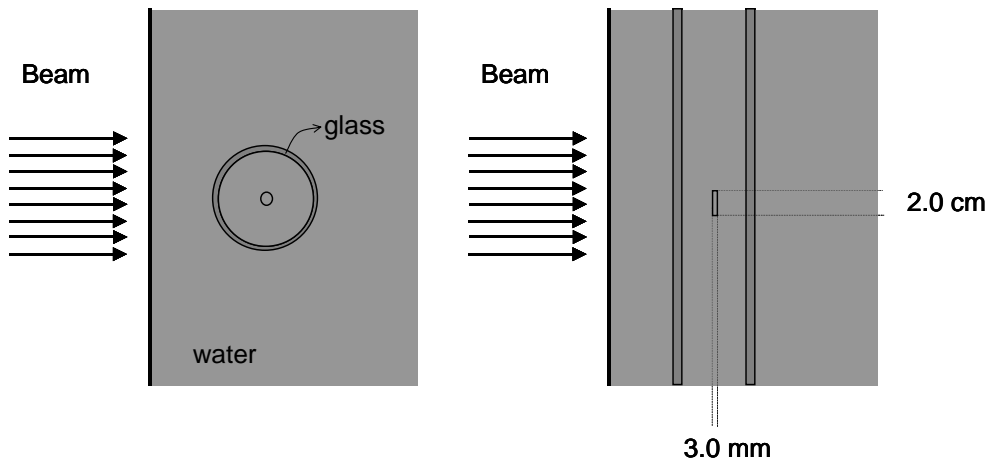


Figure 1. Geometry used in the Monte Carlo simulations as explained in the text.

### 2.1.2. Experiment

A diamond detector was used since it was the only detector available that fitted through the thermistor entry holes in the vessel. The set-up for the experiment is shown in figure 2. The diamond detector was positioned upward and well aligned with the direction of movement of the vessel. The dose response signal was first measured in the absence of the vessel, then the vessel was moved over the detector to record a second signal after which the vessel was removed and a verification signal was measured to check if the detector had not moved by a hit from the vessel. The scatter and attenuation perturbation correction factor,  $k_{sc}$ , was determined as the ratio of the response in the absence of the vessel with that in the presence of the vessel. A list of the vessels for which the experiment was performed is given in table 2. The experiment was performed for all the vessels in a  $12\text{ cm} \times 12\text{ cm}$  field since this was the standard field used at the standards laboratory at Ghent University. It was performed with a more restricted subset for other field sizes.

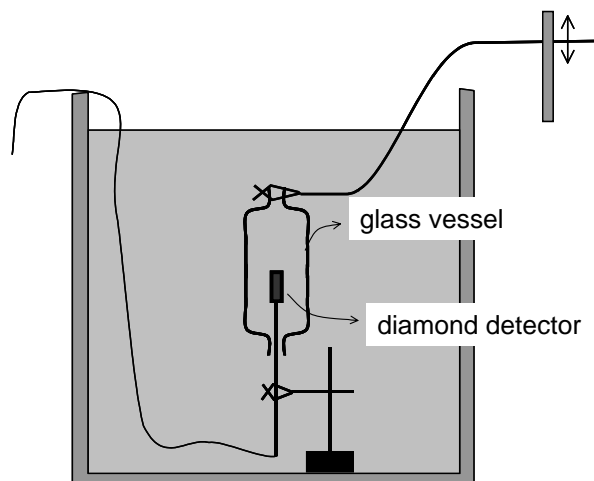


Figure 2. Experimental set-up for the measurement of  $k_{sc}$  as explained in the text.

Table 2. Dimensions of the Domen-type glass vessels used in the experimental study.

Vessel#	$\varnothing$ (mm)	$t_{\text{wall}}$ (mm)	Vessel#	$\varnothing$ (mm)	$t_{\text{wall}}$ (mm)
1	10	1.1	7	20	1.6
2	10	1.7	8	20	2.3
3	15	1.3	9	20	3.2
4	15	2.0	10	30	2.2
5	15	2.7	11	30	3.2
6	20	0.4 <sup>(*)</sup>	12	30	4.2

<sup>(\*)</sup> This is the wall thickness in the longitudinal centre of the vessel, which was not constant in thickness

## 2.2. Heat conduction

### 2.2.1. FEMLAB simulations

Heat conduction simulations were performed with FEMLAB version 2.3a [18]. This is a commercial package running under MATLAB [19] for solving partial differential equations using the finite element method. It contains pre-programmed modules for certain problems such as transient heat transfer in the chemical engineering module, which is the module used for this work. The geometries implemented in the heat conduction simulations are shown in figure 3. For the Ghent vessels, the outline of the glass vessel and probes is rotated around the central axis of the probes. The centre of the hemisphere describing the tip of the probes was considered as the point of measurement where the temperature as a function of time was calculated. The dimensions were according to the data in table 2 and the field was a square 10 cm  $\times$  10 cm field. For the calculation of the effect of one of the components separately (cylinder, probes, field), the other components were left out of the geometry. For the NPL vessel, the geometry including vessel and one probe are shown, but simulations were only done for the vessel as yet. The vessel outline was rotated around the beam axis to define its geometry. The thickness of the entrance window was 1.0 mm and all other walls were 4 mm thick. Both the diameter and the length of the vessel were 100 mm. The point of measurement was located 30 mm from the entrance window on the central axis of the cylinder. The field was a circular 10 cm diameter field and the depth dose characteristics of a  $^{60}\text{Co}$  beam were taken into account as well.

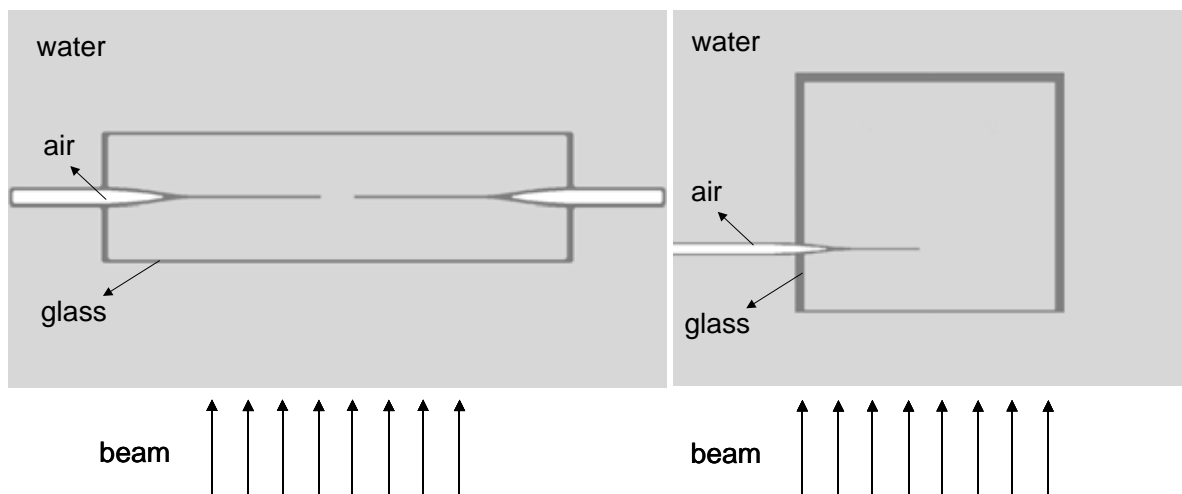


Figure 3. Top view of the geometry used in the excess heat simulations as explained in the text, for the Ghent vessels (left) and for the NPL vessels (right).

### 2.2.2. Experiment

An experiment was performed with four glass vessels of the list given in table 2. For each diameter, the vessel with the largest wall thickness was selected, i.e. vessel numbers 2, 5, 9 and 12. The largest vessel size was chosen in order to observe a maximal effect of the excess heat from the vessel, reducing the number of measurements required for a significant comparison with calculated curves. The four vessels were prepared with two of the thermistor probes used in the study by Seuntjens and Palmans [5] in the  $^{60}\text{Co}$  beam of the standards laboratory at Ghent University. The thermistors were recalibrated at NPL and even though the calibration method was different and the last calibration in Ghent took place about four years earlier, the sensitivity of one thermistor did not change more than 0.1%, whereas the second one changed over 0.2%. The vessels, with the thermistors positioned in the centre of the vessel in the direction of the beam, were cleaned with chromic acid and prepared with a filling of ultra pure water saturated with high-purity hydrogen. Both water and hydrogen were of the same quality as used in the NPL water calorimeter vessels [10]. Each vessel was subsequently mounted in the NPL water calorimeter phantom, at a depth of 5 cm in water and a source to detector distance of 80 cm where the field size was set to 10 cm  $\times$  10 cm. Irradiation times were 30 s, 60 s and 120 s.

## 3. Results and discussion

### 3.1. Scatter effects

An example of the result of the Monte Carlo calculations is given in figure 4. These were calculated for a 12 cm  $\times$  12 cm field. The statistical uncertainty on the Monte Carlo results varied between 0.05% and 0.10%.

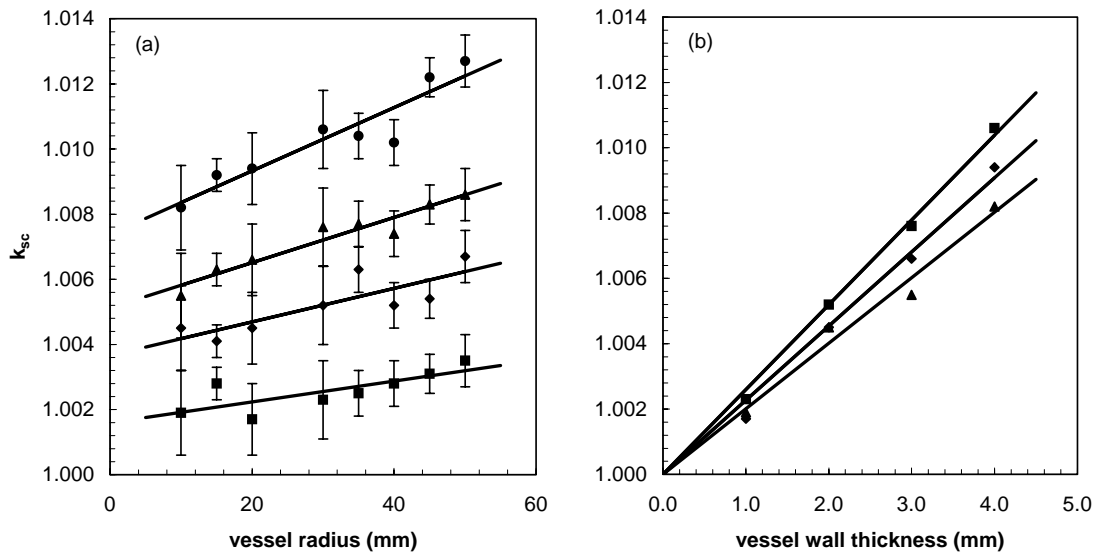


Figure 4. Results of the Monte Carlo calculations for a 12 cm  $\times$  12 cm field, (a) for vessels with wall thicknesses of 1 mm (squares), 2 mm (diamonds), 3 mm (triangles) and 4 mm (circles), plotted as a function of the vessel radius and (b) for vessels with radii of 10 mm (squares), 20 mm (diamonds) and 30 mm (triangles), plotted as a function of the vessel wall thickness. The solid lines are linear fits, which are for figure (b) forced to go through unity for a zero wall thickness. The uncertainty bars are not shown in figure (b) for clarity.

These figures show that  $k_{sc}$  can be represented by linear functions, both as a function of the wall thickness and as a function of the radius. For a standard 10 cm  $\times$  10 cm field, the results

of the Monte Carlo calculations can be summarised in a simple formula in the range of vessel dimensions specified in section 2.1.1. With  $r_{\text{vessel}}$  and  $t_{\text{wall}}$  expressed in mm, this expression is:

$$k_{\text{sc}} = 1 + 10^{-3} \cdot (0.035 \cdot r_{\text{vessel}} + 1.65) \cdot t_{\text{wall}} \quad (1)$$

A more general expression was fitted to all the Monte Carlo results in which the dimension of the field,  $a_{\text{field}}$  expressed in mm, was another parameter (so for a 12 cm  $\times$  12 cm field,  $a_{\text{field}}$  would be 120 mm):

$$k_{\text{sc}} = 1 + 10^{-3} \cdot ((0.090 - 0.00055 \cdot a_{\text{field}}) \cdot r_{\text{vessel}} + 1.65) \cdot t_{\text{wall}} \quad (2)$$

In figure 5, the results of these fits are compared with experimental data. Figure 5a compares the experiments done in Ghent using the set of vessels given in table 2 with equation (2) for a 12 cm  $\times$  12 cm field. Within the uncertainties there is a good agreement between the experimental and theoretical data, although it is not obvious (and probably not significant given the uncertainties) to resolve the differences for the different diameters from the experimental data. On the other hand, taking into consideration that the thickness of standard vessels is usually in the range below 1 mm, the differences between the various diameters in the range of 10 mm to 30 mm seem not to be very important. In figure 5b, the data from the literature given in table 1 are compared with equation (1), so this corresponds with the range of realistic vessel dimensions in standard water calorimeters. Again, the agreement is well within the uncertainties of the measurements.

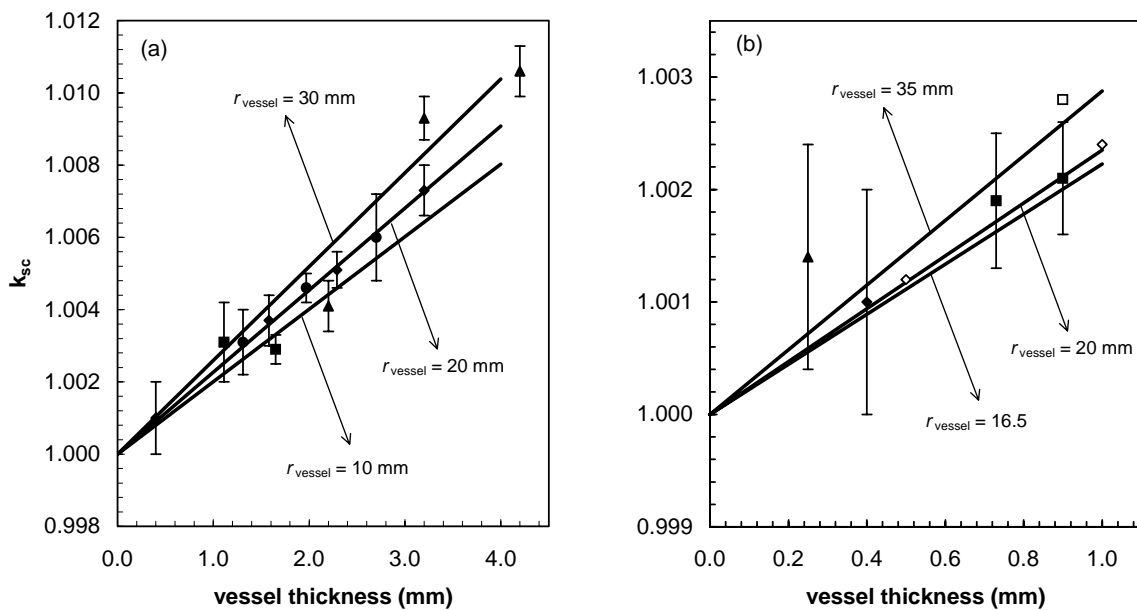


Figure 5. Comparison of  $k_{\text{sc}}$  values obtained from experiments (data points) with Monte Carlo results (solid lines). (a) Data points for the glass vessel listed in table 2 with radii of 10 mm (squares), 15 mm (circles), 20 mm (diamonds) and 30 mm (triangles). The solid lines represent equation (2) for a 12 cm  $\times$  12 cm field and three radii. (b) Data points from the literature quoted in table 1 (solid symbols are experimental data; hollow symbols are Monte Carlo data). The solid lines represent equation (1) for three radii.

### 3.2. Heat conduction

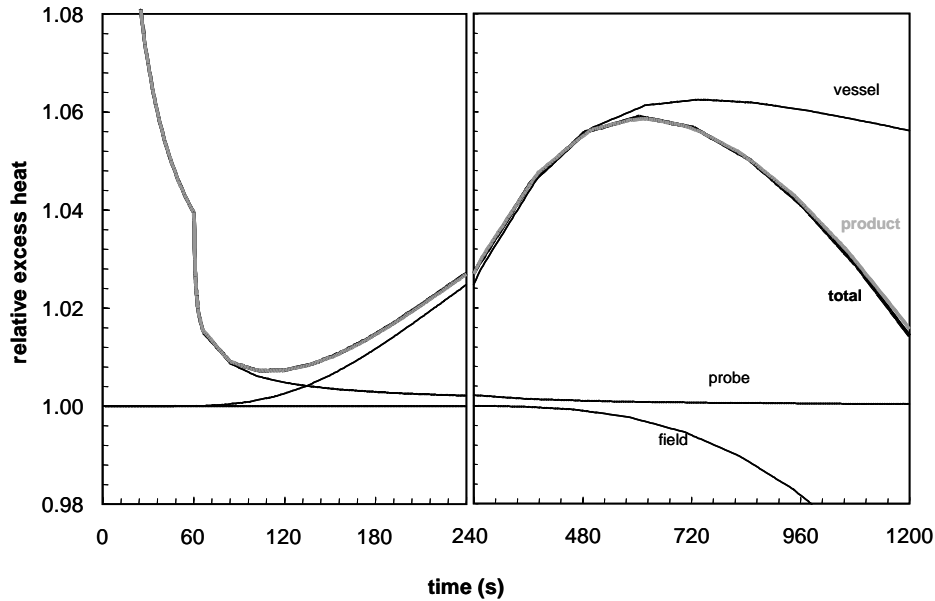


Figure 6. Excess heat at the location of the thermistor probe as a function of time for a period of 20 min after the start of the irradiation, calculated using FEMLAB. The contributions of the vessel, probe and field size are shown separately as well as the product of the three contributions.

The first numerical simulation was performed for the geometry of figure 3 with a vessel diameter of 40 mm, a vessel wall thickness of 1 mm and a probe diameter of 1 mm. The irradiation time was 60 s and dose to water in the field was 1 Gy. The temperature evolution was calculated for a post-irradiation drift time of 20 min. This calculation was mainly done to check the additivity of the various effects and the results are shown in figure 6. The excess heat plotted as a function of time is defined as the ratio of the temperature calculated at the measurement point divided by the temperature that location would have when the geometry would be homogeneous water irradiated with a uniform dose of 1 Gy. The result of the calculation with all components present is shown and compared with the product of the result for the three components (probe, vessel and field) separately. It is clear that only after a long period of time a small difference shows up between the two curves. This shows that the three components can be calculated separately such that the number of simulations required for covering a wide range of vessel and probe dimensions can be substantially reduced.

Figure 7 shows the comparison of measured post-irradiation drift curves with calculated curves for a few typical situations. Each experimental curve was an average of 6 to 12 individual curves, recorded with one thermistor probe. The simulated curves were in all cases normalised at 20s after the end of the irradiation. The pre-irradiation drift curves were 4 min for the 30 s irradiation runs and 6 min for the 60 s and 120 s irradiation runs. Prior to averaging each set of runs, the pre-irradiation drift curves were fitted linearly for each individual run. This linear fit was extrapolated up to the end of the post-irradiation drift curve and then subtracted from the complete measurement. Since post-irradiation drifts were mostly recorded for 10 min, these extrapolations cannot be very accurate and in figure 7, a quadratic fit to the residual of the pre-irradiation drift curves is shown as well. It is clear that for some measurement sets the agreement was better than for others, but there was no systematic trend in this. The differences between the measured curves and calculated curves were of the same order of magnitude as the difference between the linear and quadratic extrapolations, which

shows that the accuracy of the linear extrapolations that were performed is problematic. It must be noted that the measurements were obtained as a sequence of successive runs, such that the non-linear drifts resulting from the finite field size (see figure 6) propagate in the succeeding measurements. This effect has not been modelled in the FEMLAB calculations thus far. Another observation is that the overshoot at the start and stop of the irradiation is larger than predicted in the simulations. A possible explanation for this could be that the thermal properties of the thermistor material are very different from glass (the probe was modelled as solid glass). Krauss and Roos [9] made a similar suggestion and they derived values for the specific heat capacity and the thermal conductivity by treating these quantities as parameters, which were optimised to give an accurate agreement with measured results. Overall, the qualitative features that show up in the drift curves in figure 7, show a good agreement between the calculated and measured results, For a quantitative comparison, however, a more sophisticated analysis will be required, in which information on the drift curves is extracted from both the pre-irradiation and the post-irradiation drifts. We propose to fit the following model to the temperature as a function of time:

$$T(t) = A \cdot f(t) + a \cdot t^2 + b \cdot t + c \quad (3)$$

where  $f(t)$  is the time dependent excess heat function resulting from the FEMLAB simulations and  $A$ ,  $a$ ,  $b$  and  $c$  are parameters. If the model calculations are accurate, then  $A$  should be the same for the various vessels. A potential problem with this method could be that excess heat information in the post-irradiation drift curves is uptaken in the drift curve.

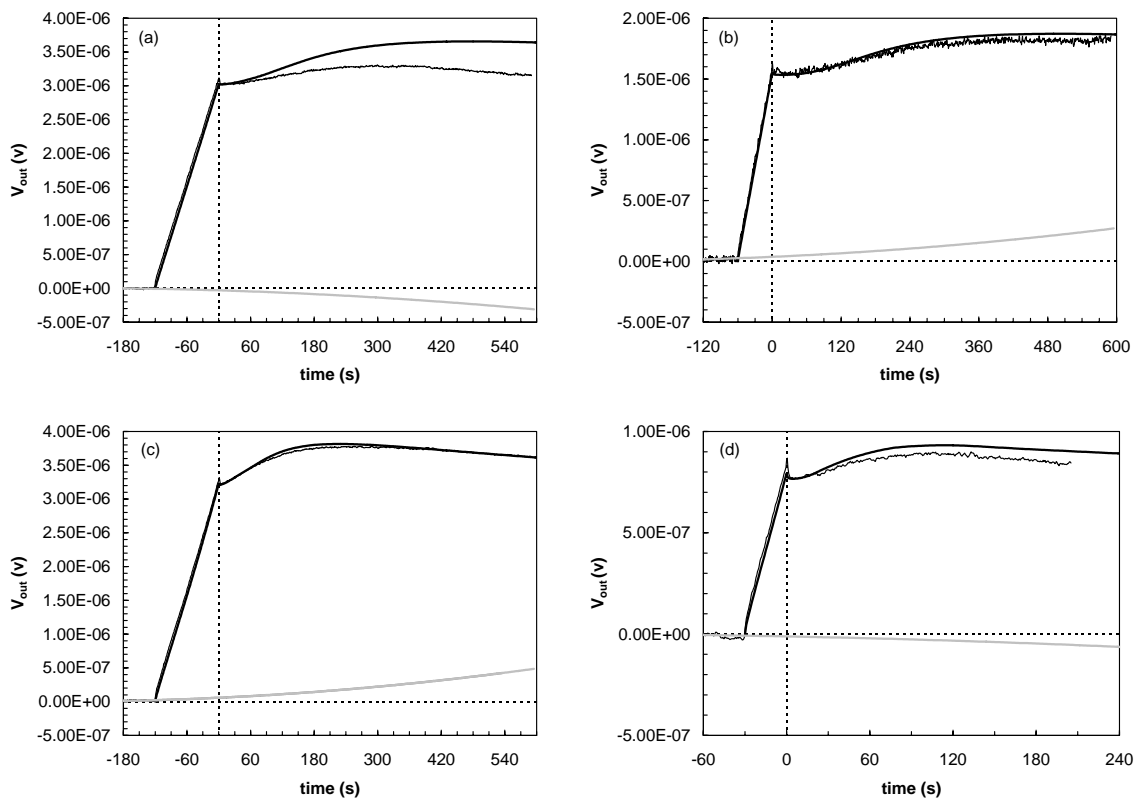


Figure 7. Measured (thin lines) and simulated drift curves (thick lines), (a) for vessel number 9 and an irradiation time of 120 s, (b) for vessel number 9 and an irradiation time of 60 s, (c) for vessel number 5 and an irradiation time of 120 s and (d) for vessel number 2 and an irradiation time of 30 s. The thick grey lines show a quadratic extrapolation of the pre-irradiation drift curves (a linear extrapolation was used in order to correct for the pre-irradiation drift).

The experimental work performed with the Ghent vessels mainly serves as a validation of the FEMLAB model calculations and will, once validated, give an indication about the accuracy of calculated results for realistic vessel dimensions for which the excess heat effect will be typically a factor ten less than the effects observed above (see references in the introduction where values can be found for Domen-type vessels). A calculated result for an NPL vessel with realistic dimensions is shown in figure 8, which also gives an idea about the magnitude of the effect for a standard vessel. The upper curve was calculated for the cylinder dimensions described in section 2.2.1, whereas for the lower curve, the diameter was slightly increased such that the field did not hit the cylindrical sidewall; thus, the difference indicates the separate effect of the sidewall. The extrapolations to mid-run result in corrections of only 0.03% for both curves, showing that with this geometry, excess heat effects are negligible. Larger effects can be expected when the thermistors are located considerably closer to the entrance window, such as in the intended future application of the calorimeter for electron beams.

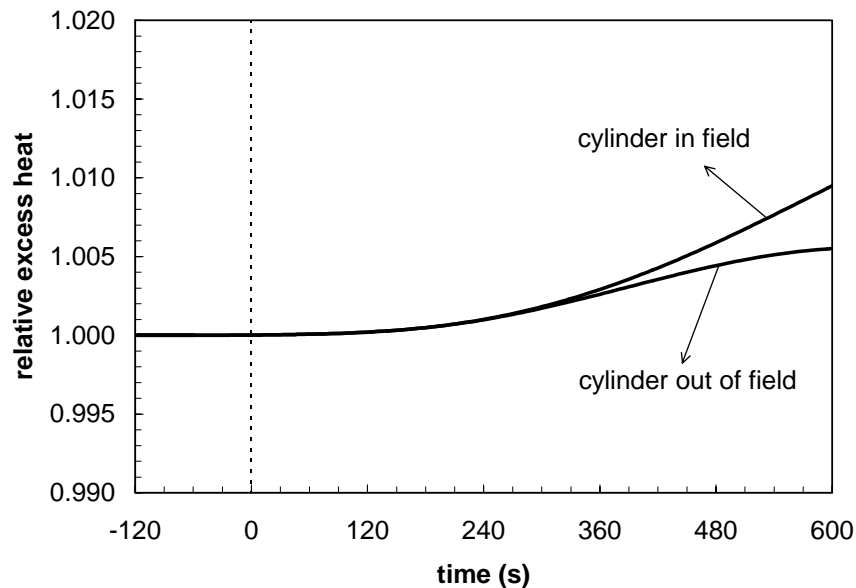


Figure 8. Excess heat for the NPL vessel as function of time relative to the end of a 120 s irradiation.

#### 4. Conclusions

Experimental and theoretical work for Domen-type and pancake type glass vessels in sealed water calorimeters has been described. For a set of Domen-type vessels with deliberately increased wall thicknesses, Monte Carlo calculations and measurements of the scatter and attenuation correction factors showed a good agreement. Based on the Monte Carlo results, a general formula with the diameter and thickness of the vessels has been proposed for a 10 cm  $\times$  10 cm square field and a second formula where the field size is an additional parameter. These theoretical results also showed a good agreement with data from the literature for realistic vessel dimensions. Four vessels out of the same set were used to measure their relative response in a  $^{60}\text{Co}$  beam and to compare these results with finite element simulations of excess heat. Qualitatively, the agreement between measurements and simulations is reasonable, but the analysis of these measurements is ongoing because the forward extrapolation of the pre-irradiation drift curves over a time period of up to 12 min (including the irradiation time) proves to be problematic. An approach has been proposed, in which information on the drifts from the post-irradiation drift curves is incorporated, which will be

used to analyse the data in the future. A simulation for a standard NPL vessel, which will be used in  $^{60}\text{Co}$ , shows that the corrections due to excess heat are very small for this vessel.

## References

- [1] Domen, S.R., *The role of water purity, convection and heat conduction in a new calorimeter design*, in Proceedings of a workshop held at the National Research Council of Canada, 6-7 June 1988, pp 85-91, NRC, Ottawa (1988).
- [2] Domen, S. R., *A Sealed Water Calorimeter for Measuring Absorbed Dose*, J. Res. Natl. Inst. Stand. Technol., **99**, 121-141 (1994).
- [3] Seuntjens, J., Van der Plaetsen, A., Van Laere, K. and Thierens, H., *Study of correction factors and the relative heat defect of a water calorimetric determination of absorbed dose to water in high energy photon beams, in Measurement Assurance in Dosimetry*. in Proceedings of a Symposium, Vienna 24-27 May 1993, pp 45-59, IAEA, Vienna (1994).
- [4] Seuntjens, J. P., Ross, C. K., Klassen, N. V. and Shortt, K.R., *A status report on the NRC sealed water calorimeter*, National Research Council of Canada Report PIRS-584, NRC, Ottawa (1999).
- [5] Seuntjens, J. and Palmans, H., *Correction factors and performance of a 4° C sealed water calorimeter*, Phys. Med. Biol., **44**, 627-646 (1999).
- [6] Aalbers, A. H. L., de Prez, L. A. and Pieksma, M. W. H., *Dosimetry of high-energy photon beams with the NMI water calorimeter*, These proceedings (2003).
- [7] Seuntjens, J., Thierens, H. and Schneider, U., *Correction factors for a cylindrical ionization chamber used in medium energy x-ray beams*, Phys. Med. Biol., **38**, 805-832 (1993).
- [8] Ross, C. K., Seuntjens, J. P., Klassen, N. V. and Shortt, K.R., *The NRC sealed water calorimeter: correction factors and performance*, in Proceedings of NPL Workshop on Recent Advances in Calorimetric Absorbed Dose Standards, Richmond 8-10 December 1999, pp 90-102, CIRM Report 42, NPL, Teddington (2000).
- [9] Krauss, A. and Roos, M., *Heat transport by material-dependent heating during absorption of radiation in the water absorbed dose calorimeter*, Thermochem. Acta, **337**, 45-49 (1999).
- [10] Williams, A. J. and Rosser, K.E., *A status report on the NPL water calorimeter*, NPL report CIRM(EXT)22, NPL, Teddington (1998).
- [11] Guerra, A. S., Laitano, R. F., Fattibene, P., Gargioni, E. and Onori, S., *The ENEA water calorimeter: characteristics and preliminary results*, in Proceedings of NPL Workshop on Recent Advances in Calorimetric Absorbed Dose Standards, Richmond 8-10 December 1999, pp 30-36, CIRM Report 42, NPL, Teddington (2000).
- [12] Palmans, H., *Experimental verification of simulated excess heat effects in the sealed water calorimeter*, in Proceedings of NPL Workshop on Recent Advances in Calorimetric Absorbed Dose Standards, Richmond 8-10 December 1999, pp 74-84, CIRM Report 42, NPL, Teddington (2000).

- [13] Domen, J. K. and Domen, S. R., *Studies of excess heat and convection in a water calorimeter*, J. Res. Natl. Inst. Stand. Technol., **106**, 843–856 (2001).
- [14] Krauss, A., *Experimental verification of calculated radiation-induced heat conduction effects in the water absorbed dose calorimeter*, Thermochem. Acta, **382**, 99-107 (2002).
- [15] Williams, A. J. and Rosser, K.E., *Development of the NPL water calorimeter*, in Proceedings of NPL Workshop on Recent Advances in Calorimetric Absorbed Dose Standards, Richmond 8-10 December 1999, pp 130-137, CIRM Report 42, NPL, Teddington (2000).
- [16] Kawrakow, I., *Accurate condensed history Monte Carlo simulation of electron transport. I EGSnrc, the new EGS4 version*, Med. Phys., **27**, 485-98 (2000).
- [17] ICRU, *Stopping powers for electrons and positrons*, International Commission on Radiation Units and Measurements Report 37, ICRU, Bethesda (1984).
- [18] Comsol AB, *FEMLAB version 2.3a*, Stockholm (2003).
- [19] The MathWorks, Inc., *MATLAB version 6.5*, Natick, MA (2002).

## Discussion

*Heather Chen-Mayer* – What is the rationale of having the two thermistors in a separate bridge rather than opposite arms of the same bridge?

*Hugo Palmans* – You can do that for two reasons. One is that one can be used as a check for the second one. If you don't find the same answer, which was the case, then it could have something to do with drifts in the tank or so on. Another aspect is that if one fails you can still go on with your measurements without losing all information. Afterwards in the analysis, if you find that one is not behaving properly, you don't have to throw away all your measurements, because you still have the other one.

*Malcolm McEwen* – Looking at those differences between your model and your measurement, and you were saying you were getting differences from one probe to the other, is that consistent differences or do you get random differences between the two probes?

*Hugo Palmans* – It is not consistent but it is always in the same direction, and it could also have to do with the asymmetry of the vessel. The vessel is not exactly symmetrical.

*Malcolm McEwen* – So there's something that's missing from the model?

*Hugo Palmans* – Yes. But that could be modelled as well.

*David Burns* – I wasn't quite sure of the use you were making of the ... lines when you did a quadratic fit to pre-irradiation data. Because if you calculate the uncertainty of an extrapolation like that, it's enormous.

*Hugo Palmans* – Yes I realise that. That's actually the way we analysed it until now, I just took the pre drift and subtracted this from the whole measured curve, but I agree that if the drift is assumed linear – and in general they are linear over quite a long time – and then you see that the residual is actually not linear, then that's probably due to the uncertainty of this extrapolation, and that will contribute to the discrepancy here. So my

main conclusion is that this is not a proper way to analyse these data and that I should do it in another way.

*David Burns* – You should put confidence limits on that fit. At the point of 230 (seconds) it will be much larger.

*Hugo Palmans* – Yes.

*Simon Duane* – Are you saying (that) there's truly a quadratic residual on that pre-drift? Or ...

*Hugo Palmans* – Yes, this is the residual.

*Malcolm McEwen* – Well if you look at the residuals on the linear fit on that front edge, is there any indication that there's a curvature to it? If you did take a quadratic, even though there's no reason to, you get something that might explain your differences.

*Hugo Palmans* – It's actually not with this one but here. I usually took 10 min time intervals (on the post drift) which are much longer than we used normally in the measurement. For a 60 second measurement, we normally used maybe intervals of 3 minutes or so. So if we used data out to this point, there would have been less of a problem.